Letter

Linearly dispersive bands at the onset of correlations in K_xC_{60} films

Ping Ai,[1] Luca Moreschini,[1,2] Ryo Mori,[1] Drew W. Latzke,[1,2] Jonathan D. Denlinger,[3] Alex Zettl,[1,2,4] Claudia Ojeda-Aristizabal,[5] and Alessandra Lanzara[1,2,*]

[1]*Materials Sciences Division, Lawrence Berkeley National Laboratory, Berkeley, California 94720, USA*
[2]*Department of Physics, University of California, Berkeley, Berkeley, California 94720, USA*
[3]*Advanced Light Source, Lawrence Berkeley National Laboratory, Berkeley, California 94720, USA*
[4]*Kavli Energy NanoSciences Institute, Berkeley, California 94720, USA*
[5]*Department of Physics and Astronomy, California State University, Long Beach, Long Beach, California 90840, USA*

(Received 1 September 2022; revised 18 March 2023; accepted 26 April 2023; published 30 May 2023)

Molecular crystals are a flexible platform to induce novel electronic phases. Due to the weak forces between molecules, intermolecular distances can be varied over larger ranges than interatomic distances in atomic crystals. On the other hand, the hopping terms are generally small, which results in narrow bands, strong correlations, and heavy electrons. Here, by growing K_xC_{60} fullerides on hexagonal layered Bi_2Se_3, we show that upon doping the series undergoes a Mott transition from a molecular insulator to a correlated metal and an in-gap state evolves into highly dispersive Dirac-like fermions at half filling, where superconductivity occurs. This picture challenges the commonly accepted description of the low-energy quasiparticles as appearing from a gradual electron doping of the conduction states and suggests an intriguing parallel with the more famous family of the cuprate superconductors. More in general, it indicates that molecular crystals offer a viable route to engineer electron-electron interactions.

DOI: 10.1103/PhysRevResearch.5.L022042

Molecular assemblies are appealing systems for engineering correlations since, intermolecular forces being typically weak, they can often be patterned in a desired way by an appropriate choice of the substrate. As a notable example, C_{60} can be grown on a number of substrates, resulting in different lattice mismatch, moiré periodicities, rotational order, and contact geometries between the C_{60} molecules [1–5]. Such flexibility allows acting on the balance between the on-site Coulomb repulsion U and the bandwidth W, thereby tuning correlations and driving qualitatively different ground states. In this sense, self-assembling molecular crystals can represent a valid alternative to the recently discovered twisted-layer structures of graphene or transition-metal dichalcogenides [6–10]. Although these have the quality of lending themselves naturally to gating experiments, the ability to select a given ground state relies on the precise control of the twist angle, which is difficult and also incompatible with any bottom-up fabrication technique, since that would necessarily privilege the rotational alignment of the layers.

Here we focus on the family of the A_xC_{60} fullerides, where fullerene molecules act as anions and other elements, often alkali metals, act as cations. The majority of the A_xC_{60} compounds are known to transition from insulating to metallic for increasing x as the C t_{1u} molecular orbitals get progressively filled [11–13]. The trivalent members are mostly metallic and superconducting, but can be antiferromagnetic insulators for large intermolecular distances. The proximity of superconductivity to a Mott insulating ground state suggested the possibility that its nature, which remains to this day uncertain, may not be that of conventional BCS theory and derive instead from electron-electron interactions, bearing similarities to the case of other unconventional superconductors [12–18].

Although the effect of electron doping by alkali metals has already been studied in many instances by photoemission, providing evidence of a clear departure from a rigid band shift [19–21], the lack of angular resolution has left many fundamental unanswered questions on how the metallic state emerges, what the nature of the low-energy excitations is, and how correlated states such as superconductivity develop from this metallic phase. Part of the difficulty associated with revealing the mechanisms behind these open questions is that, similarly to what happens in other C-based structures, such as graphene [6,22,23], the low-energy states of K_3C_{60} appear to be extremely dependent on small modifications of the crystal structure, substrate, or preparation conditions. In addition, the growth of A_xC_{60} samples is known to be prone to phase separation [24,25]. Indeed, the sparse photoemission measurements available present a remarkable variety of results for both angle-integrated [26] and angle-resolved photoemission spectroscopy (ARPES) studies, spanning from a clear hole-like dispersion reported in films grown on Ag(111) [27], to electron-like states on Ag(100) [28], to a very shallow electron pocket on Cu(111) [29].

*alanzara@lbl.gov

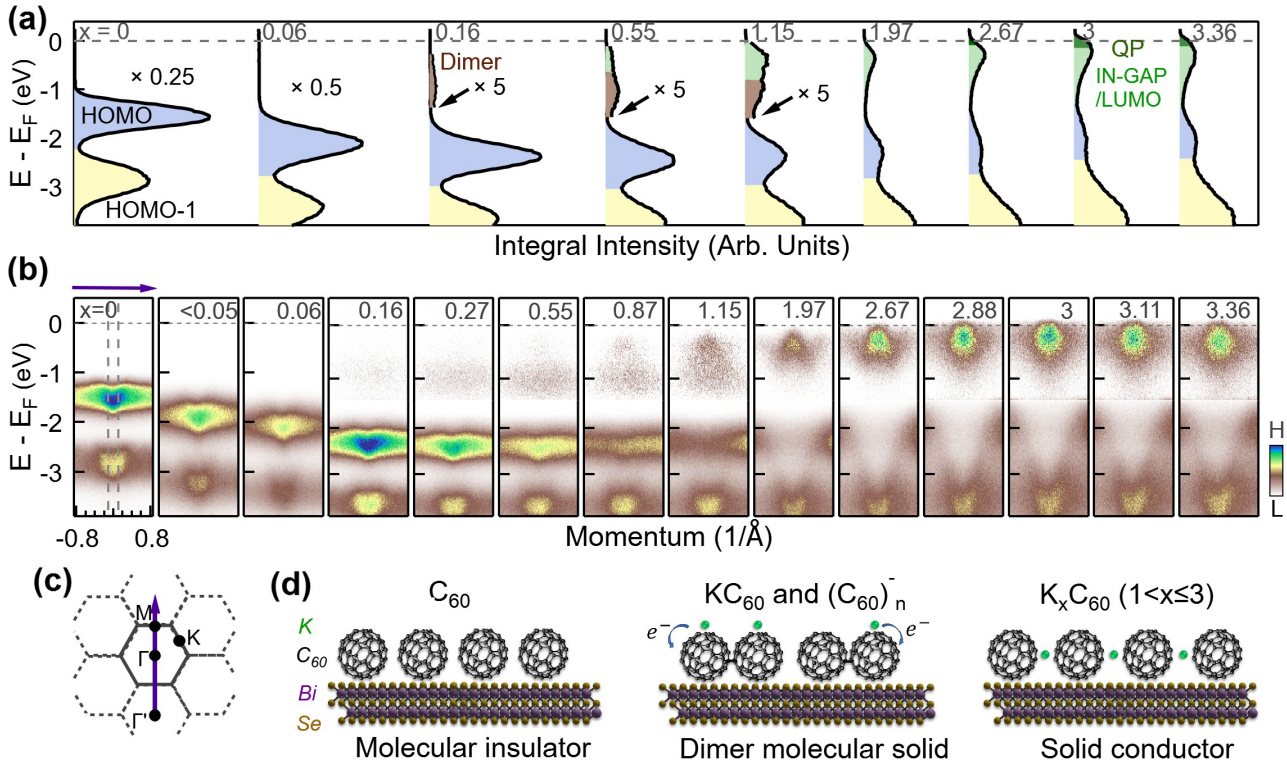

FIG. 1. (a) Photoemission intensity integrated over a narrow range at Γ, indicated by dashed lines in the leftmost panel of (b). The doping value is indicated at the top of each panel and is estimated from the intensity of the K 3*p* levels, as explained in Ref. [30]. Some curves are rescaled by the numbers indicated. The different colors indicate the approximate energy range of the electronic states described in the text. (b) ARPES dispersion in the ΓM direction, as marked in the BZ in (c). For $x > 0.06$ the intensity above and below $E = -1.4$ eV is separately rescaled by factors of 10 and 2, respectively, to enhance the signal for the low-energy states. (c) The first (solid lines) and the second BZ (dashed lines) of the sample. The green lines indicate the first BZ of Bi_2Se_3 for reference. (d) Pictorial illustration of the transition from a molecular insulator to a solid conductor with the intermediate formation of dimerized pairs. For the distance between the C_{60} molecules in the plane we assume 9.66 Å [44], which yields $\overline{\Gamma M} \simeq 0.32$ Å^{-1}.

Here, by using ARPES on *in situ* grown films, we found that when doped C_{60} molecules are deposited on top of the layered topological insulator Bi_2Se_3, a molecular subband develops, equivalent to a lower Hubbard band in a Mott scenario, accompanied by the evolution from massive to nearly massless quasiparticles as half filling is approached. These results place K_3C_{60} in the regime of correlated metals and point to the A_xC_{60} series as a platform where highly dispersive Dirac-like electrons coexist with, and possibly can be tuned or driven by, electron-electron interactions.

The samples measured in this work are K_xC_{60} films with a thickness of five monolayers grown on Bi_2Se_3(0001), as described in the methods section in [30] and in Ref. [31]. The C_{60} molecules arrange along the (111) orientation in the same fcc structure as in the bulk but with an approximately 3.4% compressed lattice. Upon doping, the alkali-metal ions progressively fill in the spaces between the buckyballs until, for $x = 3$, they form three hexagonal lattice layers for each C_{60} layer, with *abab* stacking [32]. The dispersion of the electronic bands remains mostly confined within the (111) planes (see Fig. S3 in [30]) and therefore we will discuss the data referring to the hexagonal surface Brillouin zone (BZ) of Fig. 1(c).

The evolution of the electronic structure of K_xC_{60} from the insulating C_{60} to slightly above the "optimal" metallic state at half filling ($x = 3$) is shown as a series of angle-integrated photoemission spectra in Fig. 1(a) and as ARPES maps along the ΓM direction, measured with *p* polarization, in Fig. 1(b). In the angle-integrated data, the two peaks at $x = 0$ are associated with the highest occupied molecular orbital (HOMO) and the next highest occupied molecular orbital (HOMO-1). Adding potassium, which ionizes and donates one charge per atom to the molecular solid [33], for low doping levels both the HOMO and the HOMO-1 spectral features shift toward higher binding energy as expected for a standard rigid band shift description upon electron doping, as well established from previous work [19–21]. The binding energy of the states is irrelevant in this regime since it depends on the pinning of the Fermi level E_F in the ≈1.6 eV band gap, further widened by the poor screening of the photohole [21].

For $x > 0.16$, a new in-gap state develops ≈1 eV below the Fermi level [brown in Fig. 1(a)]. Its existence only over a finite doping range $0.16 < x < 1.2$ and its separation of ≈1.2 eV from the HOMO band (measured as the peak-to-peak distance) suggests that it is related to the partial formation of C_{60} dimer pairs that can be stabilized below 270 K and prevents a simple metallic state in K_1C_{60} [34–38]. For $x > 0.5$, an additional in-gap state emerges at ≈−0.5 eV [green in Fig. 1(a)], and in parallel an overall redistribution of the spectral intensity occurs between the HOMO and

HOMO-1 bands. As we will show later [Figs. 1(b) and 3], this hybridization of the two molecular HOMO and HOMO-1 localized bands into a highly dispersive band for $x > 1.5$, much more dramatic than predicted by theory [39], marks the departure from a narrow bandwidth molecular orbital picture and the formation of a solid crystal as schematically illustrated in Fig. 1(d). As the doping approaches $x = 3$, a point which coincides with the minimum resistivity and superconductivity [20,26], the in-gap state spectral weight is maximum and it crosses the Fermi level.

While the presence of both the insulating and metallic states has been previously reported, their origin has been matter of debate for a long time [11,40,41]. Approaching the problem from band theory, the insulating phase for $x = 2, 4$ cannot be explained since the series is all expected to be metallic due to the partial filling of the t_{1u} manifold. Conversely, starting from a Mott-Hubbard approach, it is the metallic phase for $x = 3$ that is equally puzzling, since the Coulomb repulsion U is more than twice the t_{1u} bandwidth W ($\sim$0.5 eV) [42]. To unambiguously understand how metallicity develops, it is critical to have access to the energy and momentum dependence of each state upon doping of the t_{1u} manifold. We show in Fig. 1(b) such a study.

The data reveal a clear difference between the two in-gap states. Specifically, while the first one close to 1 eV is strongly localized, the second state in proximity to the Fermi level is clearly dispersive and its band velocity appears to increase approaching half filling, while its binding energy decreases (as discussed in detail later; see also Fig. S6 in [30]). This doping dependence supports an intriguing scenario where the near-E_F states are associated with the formation of a lower Hubbard band driven by correlations and are responsible for the transition to the insulating phase of a solid crystal on both sides of half filling (K_2C_{60} and K_4C_{60}). This sets the K_xC_{60} fulleride series within a Mott transition framework on both sides of $x = 3$, clearly different from the commonly accepted description where the low-energy states are assigned to a lowest unoccupied molecular orbital (LUMO)–derived band, centered above E_F, which shifts into the occupied states as the doping increases, and the transition is interpreted in a band filling picture [20,21].

The doping dependence of the near-E_F spectra is shown in Fig. 2 as an image plot of the ARPES intensity integrated over the momentum range along ΓM indicated by the red line in the inset. All the spectral features mentioned in Fig. 1 rapidly shift to higher binding energy (note the nonlinear scale for the x axis) and starting from $x \simeq 1$ they start to gradually drift back toward E_F. The shift to higher binding energies pins the Fermi level to the bottom of the unoccupied LUMO states [20,21], whereas the opposite shift [Fig. 2(b)], not as clear in previous work but evident here, is almost certainly due to the more efficient screening approaching the metallic phase compared to that in the insulating one(s).

At half filling, the quasiparticle weight also includes contributions from LUMO-derived states. In this regime the distinction between Hubbard bands and the in-gap state is of course ill-defined as the states hybridize and close the gap [43]. The fact that this doping level also corresponds to the appearance of superconductivity represents an intriguing analogy with the case of cuprates, where the Fermi surface

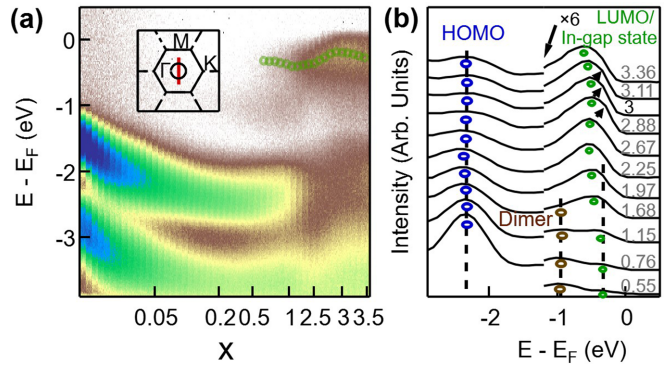

FIG. 2. (a) Detailed doping dependence of the ARPES spectra measured along ΓM, as indicated in the inset, with p-polarized light. (b) Subset of the spectra zoomed in to the in-gap, dimer, and HOMO states. The arrows for the spectra in proximity to $x = 3$ point to the shoulder of the LUMO/in-gap state peak due to the metallic quasiparticle.

is best defined in the normal state at optimal doping, at the maximum of the superconducting dome.

In Figs. 3(a) and 3(b) we compare the ARPES spectra along the ΓM direction at the two extremes of the undoped insulating phase of C_{60} and of the optimally doped metallic phase of K_3C_{60}. As discussed in Fig. 1(b), in the optimally doped phase, the merging of the C_{60} molecular electronic levels with a bandwidth of less than 0.5 eV into a single dispersive band with an overall bandwidth of nearly 2 eV for K_3C_{60} is observed. The K atoms therefore increase substantially the hopping terms between different fullerene buckyballs and the resulting bandwidth is now determined by the energy scale of the intermolecular forces [11]. Indeed, because of the hybridization between the two manifolds, the description of the orbital composition following the I_h icosahedral symmetry and the strict separation between π_5 (H-type) character for the HOMO states and π_4 (G-type) for the HOMO-1 states (Ref. [44]) is no longer valid. Such hybridization is clearly visible also in the circular dichroism signal (see Fig. S7 in [30]).

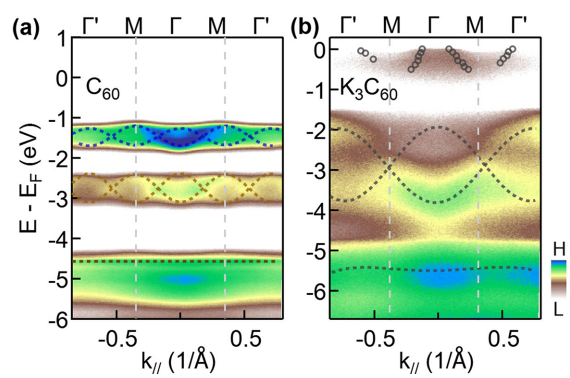

FIG. 3. (a) Band dispersion of undoped C_{60} measured with p-polarized light. The dashed curves are guides to the eye following the dispersion of the HOMO states (for details see Ref. [31]). (b) Same as (a) for K_3C_{60}. The symbols in the Fermi level region indicate the peak positions from MDC fits. Note that the energy scale in (b) is shifted by 0.7 eV relative to that in (a) to align the HOMO/HOMO1 states.

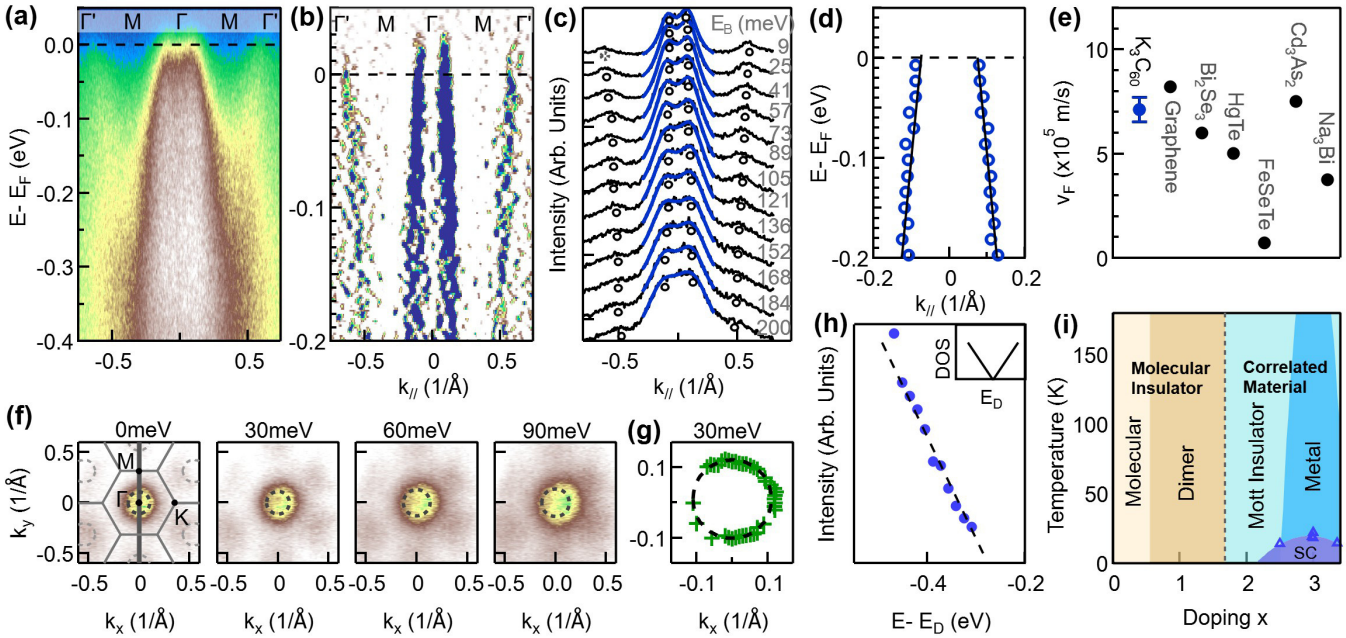

FIG. 4. Low-energy states of K_3C_{60} along ΓM shown as (a) an ARPES intensity map and (b) a second derivative plot. (c) MDC stack in the same energy region, with the binding energy in meV indicated for each spectrum. The black curves are the ARPES data, while the blue curves are best fits in a narrow energy interval around Γ by a double Lorentzian function. The circles indicate the approximate peak positions. (d) Same circles reproduced together with a fit with a power function $E_D + A|x|^b$, where E_D is the energy of the crossing point and the exponent b is not constrained. The best fit was found for $b \simeq 1.1$, very close to a linear function. The Fermi velocity from the closest linear fit is plotted in (e) together with that of several Dirac materials and, namely, graphene [23,45], Bi_2Se_3 [46], HgTe [47], $FeSe_{0.45}Te_{0.55}$ [48], Cd_3As_2 [49,50], and Na_3Bi [51]. (f) Constant energy contours at different binding energies up to 270 meV. The dashed circles in the leftmost panel mimic the contours in the second BZ. (g) Peak positions from radial fits of the constant energy contour at 30 meV. (h) Density of states as a function of the energy separation form the estimated crossing point, extracted from the integrated ARPES intensity. (i) Tentative phase diagram of K_xC_{60} as a function of doping x. The blue triangles are from Ref. [52]; we did not investigate the presence of superconductivity in our films.

At half filling an additional state can be extracted from the momentum distribution curve (MDC) fits, overlapped on the image [see markers in Fig. 3(b)], which shows holelike dispersion. At first sight it is reminiscent of the dispersive bands already reported for K_3C_{60} grown on Ag(111) [27,28], yet a side-by-side comparison (Fig. S4 in [30]) reveals that the two cases are distinct with a difference in Fermi velocity of over 70% and a band minimum shallower than 0.2 eV in Ref. [27] vs a bandwidth larger than 0.4 eV in the present study.

In Figs. 4(a) and 4(b) we report a high statistics image measured along ΓM across two BZs for $x = 3$. In contrast to the parabolic dispersion at lower doping, the data reveal a linear dispersion over the whole energy range up to 0.5 eV (see also Fig. S4 in [30]) and is reminiscent of massless Dirac fermions. The exact dispersion is extracted in a quantitative way by using a standard Lorentzian fitting of the momentum distribution curves in Figs. 4(c) and 4(d). From a linear fit of the peak positions we find a Fermi velocity $v_F = (7.1 \pm 0.6) \times 10^5$ ms^{-1}, comparable to some of the highest values reported for Dirac materials [23,45–51] [see Fig. 4(e)]. The position of the crossing point can be determined by extrapolating the dispersion to the unoccupied states and is estimated to be (0.3 ± 0.1) eV above the Fermi level. The constant energy maps (k_x vs k_y), shown in Fig. 4(f), as well as the radial MDC fits of Fig. 4(g), prove the isotropic nature of the dispersion in the surface plane. Finally, the integrated spectral weight, which is proportional to the occupied density of states, as plotted in Fig. 4(h), reveals the same linear dependence as a function of the binding energy characteristic of Dirac fermions [53], in contrast to the more parabolic dispersion at lower doping. This description holds for a narrow doping range, with a transition to a parabolic holelike dispersion for $1 < x < 2.7$ [Fig. 1(b)].

Since fullerides are widely studied materials and can be grown on a number of substrates, we are left with educated guesses of the reasons why the linearly dispersive states at Γ have not been reported before. The Bi_2Se_3 substrate used here is known to reduce the rotational disorder of the C_{60} molecules [31] and induces a compressive strain which lowers the intermolecular distance by approximately 3.4% with respect to the bulk value. This unusual situation (most substrates induce a tensile strain; see Table S1 in [30]) results in an increase of the bandwidth W, which is known to increase with the inverse of the intermolecular distance. Whereas on Ag(111) and Ag (100) values close to 0.25 eV were found [27,28],[1] here we extract a lower limit for W of 0.4 eV from the occupied portion of the t_{1u} states and up to 0.5–0.7 eV

[1]Due to the completely different fermiology, it is our best guess that the band structure reported for doped C_{60} on Cu(111) in Ref. [29] be due to an interface state and largely unrelated to the K_3C_{60} physics discussed here.

depending on the (nonaccessible) dispersion above the Fermi level. The Coulomb repulsion U, on the other hand, is less straightforward to estimate from ARPES and would require a more involved analysis and comparison with Auger spectroscopy [54]. A dedicated theoretical treatment would be welcome to determine if the increase of W is accompanied here by a lowering of the U/W ratio, which may be the culprit of the observed emergence of carriers of higher mobility at Γ. On the experimental side, a meaningful term of comparison will be provided by the recently synthesized fullerene crystals where the C_{60} molecules are covalently bonded and the intermolecular distance is reduced with respect to that in the fcc lattice [55,56].

Regardless of the microscopic origin of the Dirac-like dispersion, the results presented reveal a transition from slow and massive electrons to fast and nearly massless quasiparticles which coexist and possibly are driven by electronic correlations. These findings put forward the exciting proposal that molecular crystals, with their adaptability to be patterned on multiple substrates, and in particular A_3C_{60} compounds where even slight modifications of the bandwidth are known to result in different ground states, can provide a new flexible way to engineer correlations. In addition, the emergence of a metallic phase from an in-gap state in a fashion typical of a Mott transition hints at fascinating analogies with the case of superconducting cuprates. Interesting future developments will be to figure out how robust such massless fermions are in dependence on the intermolecular distance, as well as to explore the physics in the thin-film limit, where the moiré potential would become important. K_3C_{60} appears to be close to a sweet spot where the interplay between U and W allows for a crossover between an insulator and a correlated metal.

This work was primarily funded by the U.S. Department of Energy (DOE), Office of Science, Office of Basic Energy Sciences, Materials Sciences and Engineering Division under Contract No. DE-AC02-05-CH11231 (Ultrafast Materials Science Program No. KC2203). A.L. was partially supported as part of the Center for Novel Pathways to Quantum Coherence in Materials, an Energy Frontier Research Center funded by the DOE, Office of Science, Basic Energy Sciences. A.L. and L.M. also acknowledge support for sample growth from the Gordon and Betty Moore Foundation's EPiQS Initiative through Grant No. GBMF4859. C.O.-A. was funded for data acquisition by DOE, Office of Science, Office of Basic Energy Sciences under Contract No. DE-SC0018154. Sample growth was supported by the U.S. Department of Energy, Office of Science, Office of Basic Energy Sciences, Materials Sciences and Engineering Division under Contract No. DE-AC02-05-CH11231, within the Van der Waals Heterostructures Program No. KCWF16. The Advanced Light Source is supported by the DOE, Office of Science User Facility under Contract No. DEAC02-05CH11231.

[1] M. Kiguchi, K.-i. Iizumi, K. Saiki, and A. Koma, Atomic and electronic structures of heteroepitaxial C_{60} film grown on Ni(1 1 1), Cu(1 1 1), Appl. Surf. Sci. **212–213**, 101 (2003).

[2] L.-L. Wang and H.-P. Cheng, Rotation, translation, charge transfer, and electronic structure of C_{60} on Cu(111) surface, Phys. Rev. B **69**, 045404 (2004).

[3] K. Kim, T. H. Lee, E. J. G. Santos, P. S. Jo, A. Salleo, Y. Nishi, and Z. Bao, Structural and electrical investigation of C_{60}−graphene vertical heterostructures, ACS Nano **9**, 5922 (2015).

[4] C. Ojeda-Aristizabal, E. J. G. Santos, S. Onishi, A. Yan, H. I. Rasool, S. Kahn, Y. Lv, D. W. Latzke, J. Velasco, M. F. Crommie, M. Sorensen, K. Gotlieb, C.-Y. Lin, K. Watanabe, T. Taniguchi, A. Lanzara, and A. Zettl, Molecular arrangement and charge transfer in C_{60}/graphene heterostructures, ACS Nano **11**, 4686 (2017).

[5] N. Haag, D. Lüftner, F. Haag, J. Seidel, L. L. Kelly, G. Zamborlini, M. Jugovac, V. Feyer, M. Aeschlimann, P. Puschnig, M. Cinchetti, and B. Stadtmüller, Signatures of an atomic crystal in the band structure of a C_{60} thin film, Phys. Rev. B **101**, 165422 (2020).

[6] Y. Cao, V. Fatemi, A. Demir, S. Fang, S. L. Tomarken, J. Y. Luo, J. D. Sanchez-Yamagishi, K. Watanabe, T. Taniguchi, and E. Kaxiras, Correlated insulator behaviour at half-filling in magic-angle graphene superlattices, Nature (London) **556**, 80 (2018).

[7] Y. Cao, V. Fatemi, S. Fang, K. Watanabe, T. Taniguchi, E. Kaxiras, and P. Jarillo-Herrero, Unconventional superconductivity in magic-angle graphene superlattices, Nature (London) **556**, 43 (2018).

[8] M. M. Ugeda, A. J. Bradley, S.-F. Shi, H. Felipe, Y. Zhang, D. Y. Qiu, W. Ruan, S.-K. Mo, Z. Hussain, Z.-X. Shen, Giant bandgap renormalization and excitonic effects in a monolayer transition metal dichalcogenide semiconductor, F. Wang, S. G. Louie, and M. F. Crommie, Nat. Mater. **13**, 1091 (2014).

[9] L. Wang, E.-M. Shih, A. Ghiotto, L. Xian, D. A. Rhodes, C. Tan, M. Claassen, D. M. Kennes, Y. Bai, B. Kim, K. Watanabe, T. Taniguchi, X. Zhu, J. Hone, A. Rubio, A. N. Pasupathy, and C. R. Dean, Correlated electronic phases in twisted bilayer transition metal dichalcogenides, Nat. Mater. **19**, 861 (2020).

[10] Y. Xu, C. Horn, J. Zhu, Y. Tang, L. Ma, L. Li, S. Liu, K. Watanabe, T. Taniguchi, J. C. Hone, J. Shan, and K. F. Mak, Creation of moiré bands in a monolayer semiconductor by spatially periodic dielectric screening, Nat. Mater. **20**, 645 (2021).

[11] O. Gunnarsson, Superconductivity in fullerides, Rev. Mod. Phys. **69**, 575 (1997).

[12] M. Capone, M. Fabrizio, C. Castellani, and E. Tosatti, *Colloquium:* Modeling the unconventional superconducting properties of expanded A_3C_{60} fullerides, Rev. Mod. Phys. **81**, 943 (2009).

[13] Y. Takabayashi and K. Prassides, Unconventional high-T_c superconductivity in fullerides, Philos. Trans. R. Soc. A **374**, 20150320 (2016).

[14] M. Capone, M. Fabrizio, C. Castellani, and E. Tosatti, Strongly correlated superconductivity, Science **296**, 2364 (2002).

[15] P. Durand, G. R. Darling, Y. Dubitsky, A. Zaopo, and M. J. Rosseinsky, The MottHubbard insulating state and orbital degeneracy in the superconducting C_{60}^{3-} fulleride family, Nat. Mater. **2**, 605 (2003).

[16] N. Manini and E. Tosatti, Theoretical aspects of highly correlated fullerides: metal-insulator transition, arXiv:cond-mat/0602134.

[17] F. Steglich and S. Wirth, Foundations of heavy-fermion superconductivity: Lattice Kondo effect and Mott physics, Rep. Prog. Phys. **79**, 084502 (2016).

[18] H. M. Yamamoto, Phase-transition devices based on organic Mott insulators, Bull. Chem. Soc. Jpn. **94**, 2505 (2021).

[19] C. T. Chen, L. Tjeng, P. Rudolf, G. Meigs, J. Rowe, J. Chen, J. McCauley, A. Smith, A. McGhie, and W. Romanow, Electronic states and phases of K_xC_{60} from photoemission and X-ray absorption spectroscopy, Nature (London) **352**, 603 (1991).

[20] M. Merkel, M. Knupfer, M. S. Golden, J. Fink, R. Seemann, and R. L. Johnson, Photoemission study of the electronic structure of C_{60} and K_xC_{60}, Phys. Rev. B **47**, 11470 (1993).

[21] G. K. Wertheim and D. N. E. Buchanan, Bulk and surface electronic structures of potassium fullerides, Phys. Rev. B **47**, 12912 (1993).

[22] J. L. McChesney, A. Bostwick, T. Ohta, T. Seyller, K. Horn, J. González, and E. Rotenberg, Extended van Hove Singularity and Superconducting Instability in Doped Graphene, Phys. Rev. Lett. **104**, 136803 (2010).

[23] C. Hwang, D. A. Siegel, S.-K. Mo, W. Regan, A. Ismach, Y. Zhang, A. Zettl, and A. Lanzara, Fermi velocity engineering in graphene by substrate modification, Sci. Rep. **2**, 590 (2012).

[24] S. Kawasaki, J. Fukui, T. Motoyama, Y. Suzuki, S. Shibasaki, and G.-q. Zheng, The Mott state and superconductivity in face-centred cubic structured Cs_3C_{60}: A ^{133}Cs-nuclear magnetic resonance study under pressure, J. Phys. Soc. Jpn. **82**, 014709 (2013).

[25] V. Brouet, W. Yang, X. Zhou, Z. Hussain, and Z. Shen, Dependence of the band structure of C_{60} monolayers on molecular orientations and doping observed by angle resolved photoemission, J. Phys. Chem. Solids **67**, 218 (2006).

[26] R. Hesper, L. H. Tjeng, A. Heeres, and G. A. Sawatzky, Photoemission evidence of electronic stabilization of polar surfaces in K_3C_{60}, Phys. Rev. B **62**, 16046 (2000).

[27] W. Yang, V. Brouet, X. Zhou, H. J. Choi, S. G. Louie, M. L. Cohen, S. Kellar, P. Bogdanov, A. Lanzara, and A. Goldoni, Band structure and fermi surface of electron-doped C_{60} monolayers, Science **300**, 303 (2003).

[28] V. Brouet, W. L. Yang, X. J. Zhou, H. J. Choi, S. G. Louie, M. L. Cohen, A. Goldoni, F. Parmigiani, Z. Hussain, and Z. X. Shen, Orientation-Dependent C_{60} Electronic Structures Revealed by Photoemission Spectroscopy, Phys. Rev. Lett. **93**, 197601 (2004).

[29] W. W. Pai, H. T. Jeng, C.-M. Cheng, C.-H. Lin, X. Xiao, A. Zhao, X. Zhang, G. Xu, X. Q. Shi, M. A. Van Hove, C.-S. Hsue, and K.-D. Tsuei, Optimal Electron Doping of a C_{60} Monolayer on Cu(111) via Interface Reconstruction, Phys. Rev. Lett. **104**, 036103 (2010).

[30] See Supplemental Material at http://link.aps.org/supplemental/10.1103/PhysRevResearch.5.L022042 for materials and methods, additional characterization data and a summary of reported reconstructions of C_{60} on various substrates.

[31] D. W. Latzke, C. Ojeda-Aristizabal, S. M. Griffin, J. D. Denlinger, J. B. Neaton, A. Zettl, and A. Lanzara, Observation of highly dispersive bands in pure thin film C_{60}, Phys. Rev. B **99**, 045425 (2019).

[32] P. W. Stephens, L. Mihaly, P. L. Lee, R. L. Whetten, S.-M. Huang, R. Kaner, F. Deiderich, and K. Holczer, Structure of single-phase superconducting K_3C_{60}, Nature (London) **351**, 632 (1991).

[33] J. L. Martins and N. Troullier, Structural and electronic properties of K_nC_{60}, Phys. Rev. B **46**, 1766 (1992).

[34] Q. Zhu, D. E. Cox, and J. E. Fischer, Phase transitions in KC_{60}: Dimer formation via rapid quenching, Phys. Rev. B **51**, 3966 (1995).

[35] G. Oszlányi, G. Bortel, G. Faigel, M. Tegze, L. Gránásy, S. Pekker, P. W. Stephens, G. Bendele, R. Dinnebier, G. Mihály, A. Jánossy, O. Chauvet, and L. Forró, Dimerization in KC_{60} and RbC_{60}, Phys. Rev. B **51**, 12228 (1995).

[36] T. Pichler, M. Knupfer, M. S. Golden, S. Haffner, R. Friedlein, J. Fink, W. Andreoni, A. Curioni, M. Keshavarz-K, C. Bellavia-Lund, A. Sastre, J.-C. Hummelen, and F. Wudl, On-Ball Doping of Fullerenes: The Electronic Structure of C_{59}N Dimers from Experiment and Theory, Phys. Rev. Lett. **78**, 4249 (1997).

[37] R. Macovez, P. Rudolf, I. Marenne, L. Kjeldgaard, P. A. Brühwiler, T. Pichler, P. Vilmercati, R. Larciprete, L. Petaccia, G. Bertoni, and A. Goldoni, Electronic surface reconstruction and correlation in the fcc and dimer phases of RbC_{60}, Phys. Rev. B **75**, 195424 (2007).

[38] D. Konarev, S. Khasanov, A. Otsuka, M. Maesato, G. Saito, and R. Lyubovskaya, A two-dimensional organic metal based on fullerene, Angew. Chem. Int. Ed. **49**, 4829 (2010).

[39] S. C. Erwin and W. E. Pickett, Theoretical fermi-surface properties and superconducting parameters for K_3C_{60}, Science **254**, 842 (1991).

[40] O. Gunnarsson, E. Koch, and R. M. Martin, Mott transition in degenerate Hubbard models: Application to doped fullerenes, Phys. Rev. B **54**, R11026 (1996).

[41] J. E. Han, E. Koch, and O. Gunnarsson, Metal-Insulator Transitions: Influence of Lattice Structure, Jahn-Teller Effect, and Hund's Rule Coupling, Phys. Rev. Lett. **84**, 1276 (2000).

[42] S. Satpathy, V. P. Antropov, O. K. Andersen, O. Jepsen, O. Gunnarsson, and A. I. Liechtenstein, Conduction-band structure of alkali-metal-doped C_{60}, Phys. Rev. B **46**, 1773 (1992).

[43] Y. Wang, Y. He, K. Wohlfeld, M. Hashimoto, E. W. Huang, D. Lu, S.-K. Mo, S. Komiya, C. Jia, B. Moritz, Z.-X. Shen, and T. P. Devereaux, Emergence of quasiparticles in a doped Mott insulator, Commun. Phys. **3**, 210 (2020).

[44] D. W. Latzke, C. Ojeda-Aristizabal, J. D. Denlinger, R. Reno, A. Zettl, and A. Lanzara, Orbital character effects in the photon energy and polarization dependence of pure C_{60} photoemission, ACS Nano **13**, 12710 (2019).

[45] A. H. Castro Neto, F. Guinea, N. M. R. Peres, K. S. Novoselov, and A. K. Geim, The electronic properties of graphene, Rev. Mod. Phys. **81**, 109 (2009).

[46] Y. Xia, D. Qian, D. Hsieh, L. Wray, A. Pal, H. Lin, A. Bansil, D. Grauer, Y. S. Hor, R. J. Cava, and M. Z. Hasan, Observation of a large-gap topological-insulator class with a single Dirac cone on the surface, Nat. Phys. **5**, 398 (2009).

[47] M. König, S. Wiedmann, C. Brüne, A. Roth, H. Buhmann, L. W. Molenkamp, X.-L. Qi, and S.-C. Zhang, Quantum spin Hall insulator state in HgTe quantum wells, Science **318**, 766 (2007).

[48] P. Zhang, K. Yaji, T. Hashimoto, Y. Ota, T. Kondo, K. Okazaki, Z. Wang, J. Wen, G. D. Gu, H. Ding, and S. Shin, Observation of topological superconductivity on the surface of an iron-based superconductor, Science **360**, 182 (2018).

[49] S. Borisenko, Q. Gibson, D. Evtushinsky, V. Zabolotnyy, B. Büchner, and R. J. Cava, Experimental Realization of a Three-Dimensional Dirac Semimetal, Phys. Rev. Lett. **113**, 027603 (2014).

[50] M. Neupane, S.-Y. Xu, R. Sankar, N. Alidoust, G. Bian, C. Liu, I. Belopolski, T.-R. Chang, H.-T. Jeng, H. Lin, A. Bansil, F. Chou, and M. Z. Hasan, Observation of a three-dimensional topological Dirac semimetal phase in high-mobility Cd_3As_2, Nat. Commun. **5**, 3786 (2014).

[51] Z. K. Liu, B. Zhou, Y. Zhang, Z. J. Wang, H. M. Weng, D. Prabhakaran, S.-K. Mo, Z. X. Shen, Z. Fang, X. Dai, Z. Hussain, and Y. L. Chen, Discovery of a three-dimensional topological dirac semimetal, Na_3Bi, Science **343**, 864 (2014).

[52] M.-Q. Ren, S. Han, S.-Z. Wang, J.-Q. Fan, C.-L. Song, X.-C. Ma, and Q.-K. Xue, Direct Observation of Full-Gap Superconductivity and Pseudogap in Two-Dimensional Fullerides, Phys. Rev. Lett. **124**, 187001 (2020).

[53] S. Zhou, G.-H. Gweon, J. Graf, A. Fedorov, C. Spataru, R. Diehl, Y. Kopelevich, D.-H. Lee, S. G. Louie, and A. Lanzara, First direct observation of Dirac fermions in graphite, Nat. Phys. **2**, 595 (2006).

[54] R. W. Lof, M. A. van Veenendaal, B. Koopmans, H. T. Jonkman, and G. A. Sawatzky, Band gap, excitons, and Coulomb interaction in solid C_{60}, Phys. Rev. Lett. **68**, 3924 (1992).

[55] L. Hou, X. Cui, B. Guan, S. Wang, R. Li, Y. Liu, D. Zhu, and J. Zheng, Synthesis of a monolayer fullerene network, Nature (London) **606**, 507 (2022).

[56] E. Meirzadeh, A. M. Evans, M. Rezaee, M. Milich, C. J. Dionne, T. P. Darlington, S. T. Bao, A. K. Bartholomew, T. Handa, D. J. Rizzo, R. A. Wiscons, M. Reza, A. Zangiabadi, N. Fardian-Melamed, A. C. Crowther, P. J. Schuck, D. N. Basov, X. Zhu, A. Giri, P. E. Hopkins *et al.*, A few-layer covalent network of fullerenes, Nature (London) **613**, 71 (2023).